First report of the MILESTONE experiment: strongly stratified turbulence and mixing efficiency in the Coriolis platform

Antoine Campagne[1], Henrik Alfredsson[2], Rémi Chassagne[1], Diane Micard[3], Nicolas Mordant[1], Antonio Segalini[2], Joel Sommeria[1], Samuel Viboud[1], Ashwin Vishnu Mohanan[2], Erik Lindborg[2] and Pierre Augier[1]

[1]LEGI, Université Grenoble Alpes, CNRS, France
[2]Royal Institute of Technology (KTH), Department of Mechanics, Stockholm, Sweden
[3]LMFA, École Centrale de Lyon, France
Antoine.Campagne@univ-grenoble-alpes.fr

Abstract

Strongly stratified turbulence is a possible interpretation of oceanic and atmospheric measurements. However, this regime has never been produced in a laboratory experiment because of the two conditions of very small horizontal Froude number F_h and large buoyancy Reynolds number $\mathcal{R}$ which require a verily large experimental facility. We present a new attempt to study strongly stratified turbulence experimentally in the Coriolis platform. The flow is forced by a slow periodic movement of an array of six vertical cylinders of 25 cm diameter with a mesh of 75 cm. Five cameras are used for 3D-2C scanned horizontal particles image velocimetry (PIV) and stereo 2D vertical PIV. Five density-temperature probes are used to measure vertical and horizontal profiles and signals at fixed positions. The first preliminary results indicate that we manage to produce strongly stratified turbulence at very small F_h and large $\mathcal{R}$ in a laboratory experiment.

1 Introduction

Our understanding of the dynamics of turbulence strongly influenced by a stable density stratification has been deeply changed at the beginning of the 21st century. Studies based on large-resolution numerical simulations have shown that there is a strongly stratified regime associated with a downscale energy cascade (Riley and de Bruyn Kops, 2003; Lindborg, 2006). It has been understood that the stratified turbulence is characterised by two important non-dimensional numbers and that the regime called "strongly stratified turbulence" is obtained only for very small horizontal Froude number and large buoyancy Reynolds number (Billant and Chomaz, 2001; Brethouwer et al., 2007),

$$F_h = \frac{\varepsilon_K}{NU^2} \ll 1, \quad \mathcal{R} = \frac{\varepsilon_K}{\nu N^2} > 10, \tag{1}$$

where ε_K is the kinetic energy dissipation, N the Brunt-Väissälä frequency, U the root-mean-square horizontal velocity and ν the kinematic viscosity. Riley and Lindborg (2008) showed that strongly stratified turbulence is a possible interpretation for some geophysical turbulent measurements.

In a laboratory experiment, it is very difficult to fulfill the two conditions $F_h \ll 1$ and $\mathcal{R} > 10$ at the same time, since this requires very large facilities. Most of stratified flows studied experimentally correspond to a regime very different than strongly stratified geophysical flows (see for example Praud et al., 2005; Augier et al., 2014, 2015). Brethouwer and Lindborg (2009) and Maffioli and Davidson (2016) investigated numerically the mixing produced by strongly stratified turbulence and showed that at very small horizontal

Froude number ($F_h < 0.03$) and large buoyancy Reynolds number, the mixing efficiency tends to be independent of these parameters with a mixing coefficient $\Gamma = \varepsilon_A/\varepsilon_K$ of the order of 0.35, where ε_A and ε_K are the dissipation rates of available potential energy and kinetic energy, respectively. This value is nearly twice larger that the canonical value 0.2 used for mixing parametrization in oceanic models. Moreover, the effect of rotation on mixing efficiency of strongly stratified turbulence has to be investigated.
We present the first report of the EuHIT project experiment (called MILESTONE) dedicated to better understand these issues by careful measurements of strongly stratified turbulence in a large-scale experiment in the Coriolis platform.

2 Experimental setup

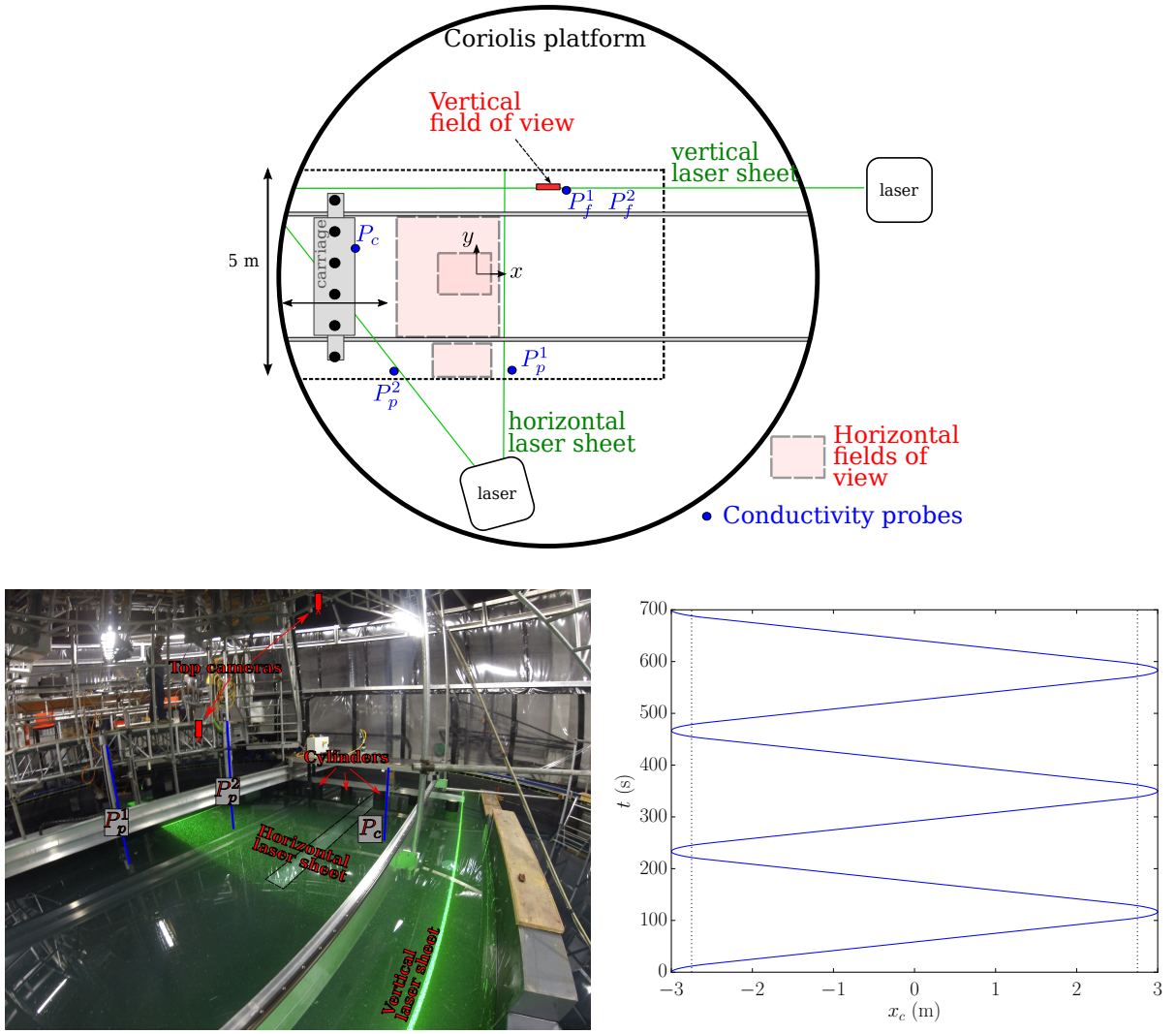

Figure 1: Top: scheme of the experimental setup (see text for description). Bottom left: photography of the experiment. Two of our cameras are visible (highlighted in red), the third one being below the window highlighted by the black rectangle. Three of our five probes are highlighted in blue, P_c is embarked on the carriage and P_p^1 and P_p^2 are attached to profilers. The vertical PIV field of view and its associated cameras are not visible in the photo. Bottom right: chronogram of the position of the carriage $x_c(t)$.

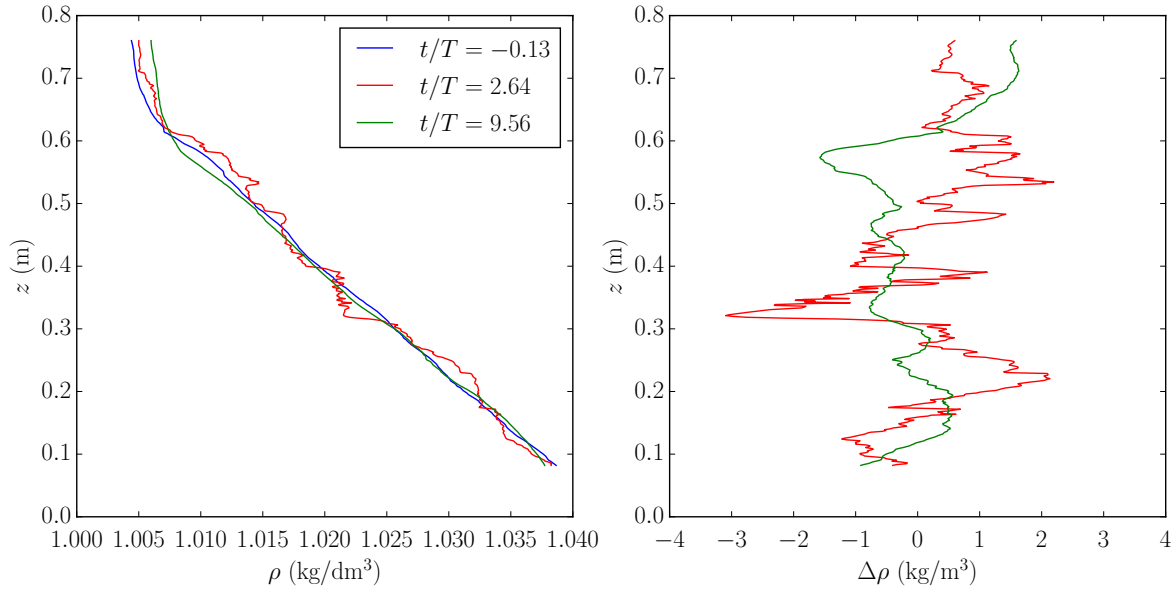

Figure 2: Left: density profiles for $N = 0.8$ rad/s and $U_c = 6$ cm/s. Right: variations of density with respect to the profile at rest $\Delta\rho = \rho - \rho(t/T = -0.13)$.

2.1 Overview of the experiment

The experimental setup, installed in the large Coriolis platform, is presented in figure 1: a tank with a rectangle base of 9×6 m^2 area is filled with an approximately linear salt stratification of 81 cm depth. The flow is generated with an oscillating comb consisting of 6 vertical cylinders of 25 cm diameter attached to a carriage with a mesh of $M = 75$ cm. We impose on the carriage the following periodic motion of period T (see figure 4 for a chronogram of its position x_c): it accelerates with a constant acceleration over 25 cm to a velocity U_c, travels at the uniform speed a distance of 550 cm and decelerates with a constant deceleration over 25 cm. It them comes back to its initial position with the opposite movement and immediately restarts this cycle. In the following, we use cartesian coordinates with the origin centered with respect to the vertical walls and at the bottom of the tank. The vertical coordinate is given by z and the horizontal coordinate along the direction of displacement of the carriage by x such that (x, y, z) form right handed coordinates.

We performed a large number of experiments varying the velocity U_c of the carriage and the linear stratification characterized by the Brunt-Väissälä frequency

$$N = \sqrt{-\frac{g}{\langle\rho\rangle_z}\frac{\partial\rho}{\partial z}}, \tag{2}$$

where g denotes the gravitational acceleration, ρ the volumetric mass density of the fluid and $\langle\cdot\rangle_z$ the vertical average. In practice, N is evaluated from the density profile $\rho(z)$ measured at rest, the slope $\partial\rho/\partial z$ being computed by a linear fit over $\rho(z)$ on 20 cm around the mid-height of water. A single experiment can be characterized by two dimensionless parameters based on the forcing control parameters, a horizontal Froude number and a buoyancy Reynolds number, defined as

$$F_{hc} = \frac{U_c}{NM}, \quad \mathcal{R}_c = \frac{{U_c}^3}{\nu N^2 M}. \tag{3}$$

Table 1: Parameters explored in our experiments without system rotation. The line written in bold font indicates the experiment described in the last section of the present paper. F_{hc} and $\mathcal{R}_c$ are based on the carriage velocity U_c and the mesh M as defined in equations (3). F_{he} and $\mathcal{R}_e$ are estimations of the turbulent Froude and buoyancy Reynolds numbers as defined in equations (1) and (6), i.e. with the estimations $E_K \simeq 0.08 U_c^2$ and $\varepsilon_K \simeq 0.02 {U_c}^3/M$.

N (rad/s)	U_c (cm/s)	F_{hc}	$\mathcal{R}_c$	F_{he}	$\mathcal{R}_e$
0	[2, 4, 6, 8, 12, 16]	∞	∞	∞	∞
0.4	2	0.07	67	0.02	1.3
	4	0.13	533	0.03	10.7
	6	0.20	1800	0.05	36.0
	8	0.27	4267	0.07	85.3
	12	0.40	14400	0.10	288.0
	16	0.53	34133	0.13	682.7
0.8	2	0.03	17	0.01	0.3
	4	0.07	133	0.02	2.7
	6.00	**0.10**	**450**	**0.02**	**9.0**
	8	0.13	1067	0.03	21.3
	12	0.20	3600	0.05	72.0
	16	0.27	8533	0.07	170.7

Table 1 presents the parameters spanned with the experiments performed without rotation. Thanks to the large dimensions of our facility, we obtain small to moderate Froude numbers $F_{hc} \in [0.03,\ 0.53]$ and small to large buoyancy Reynolds numbers $\mathcal{R}_c \in [15,\ 34133]$. Analysis on scaling laws with respect to F_{hc} and $\mathcal{R}_c$ is of course needed for a careful understanding of the flows. However, as this project is at its earliest stage, a thorough analysis has not yet been done. For the sake of simplicity, we only present here preliminary results from the case for $F_{hc} = 0.1$ and $\mathcal{R}_c = 450$ (highlighted by bold font in table 1).

2.2 Measurements

This experiment benefits from a well-furnished instrumentation which is described in the following.

Density measurements Five calibrated conductimetric probes P_i^j measure the volumetric mass density (see figure 1). The probe P_c is embarked on the carriage at the position $(x_c(t) + 0.48,\ 0.71,\ 0.395)$ m. Since the position of this probe breaks the symetry with respect to the x-axis, its signal has to be separated into two phases. When the probe is downstream, the measurement can be interpreted as the statistically stationary signal of a forced turbulence. When the probe is upstream, we can suppose that the probe is not affected by the cylinders. The measurement can then be interpreted as the signal of the decaying turbulence that has been generated during the previous phase.
The probes P_f^1 and P_f^2 are respectively placed near the bottom $(2.73, 2.18, 0.025)$ m and near the surface $(2.73, 2.18, 0.785)$ m in order to measure the time evolution of the mixed layers. Finally, the probes P_p^1 and P_p^2 are fixed on well controlled vertical profilers at positions $(-1.01, 2.24, z_p(t))$ and $(1.66, 2.14, z_p(t))$, respectively. The short time response of the probes and the rapidity of the profilers allow us to get well resolved vertical density

profiles over 70 cm height on a time of 8 s. Figure 2 represents three density profiles during an experiment consisting of 7 periods of oscillation of the carriage. The blue line corresponds to the background profile with fluid at rest. It shows a well defined linear dependence below $z = 65$ cm and a mixed layer near the surface. The expected mixed layer at the bottom is not present here since the probes does not approach enough the bottom of the tank. Profiles at later times show density fluctuations with respect to the background profile of the order of 1 kg/m^3 which corresponds to a typical vertical displacement of isopycnals of 1 cm. In the profile for $t/T = 9.56$ (yellow curves), we see that part of these fluctuations persist a long time after the carriage stops. Importantly, we see that we can easily measure the density variation in time at the surface that will allow us to compute the mixing efficiency for every experiment.

PIV measurements We measure vertical and horizontal velocity fields using two PIV systems. The vertical measurement domain is a 0.45×0.45 m^2 vertical square with a resolution of 5 mm centered at the position $(1.88, 2.20, 0.35)$ m. We acquire up to 1300 images per period of oscillation T with a 1024^2 pixel camera.
Horizontal fields are measured with 2D scanned PIV system with a rapid vertically oscillating horizontal laser sheet. The vertical position of the laser sheet is given by a staircase profile with up to 11 levels on a time less than 100 ms. Oscillation of the laser sheet is achieved by an oscillating mirror placed 6 m from the region of interest. Half of the depth can be scanned with quasi-horizontal laser sheets, with the angle of the laser sheet with respect to the horizontal being less than 1.5°. In practice, two sets of measurement are done: one with a small scan amplitude (five planes with $z \in [0.483,\ 0.514]$ m) in order to resolve small vertical scale structures. The second set is performed with a large scan amplitude (typically eight planes with $z \in [0.252,\ ,0.554]$ m) that provides more vertically decorrelated fields. Images are acquired by three 2560×2160 pixel cameras synchronized with the oscillating mirror, each camera looking on three different regions of interest (see figure 1). Two of them are centered at $y = 0$ with a large and a small field. The larger field (2.2×2.5 m^2) is acquired from the top through the water surface and the small field (1.18×0.53 m^2) through a glass from the bottom of the tank. The third view (1.3×1.0 m^2) is taken at the vicinity of a side wall. We acquire up to 1300 images per vertical level of the laser sheet and per period of the movement of the cylinders.
Acquisition of images begins after one period of oscillation of the carriage and ends one period after the carriage stops. The forcing consists of 3 periods of oscillation for the small amplitude scan case and 12 periods for large scan amplitude case.
Figure 3 shows instantaneous horizontal and vertical velocity fields for $t/T = [1.31,\ 1.5,\ 1.68]$. The resolution is equal to 5.3 mm for the vertical cross-section and 2.3 cm for the horizontal cross-section. Note that, as the turbulence is inhomogeneous and positions of measurement of horizontal and vertical fields are different, these former fields cannot be mutually described. Just after the carriage quit the field of view of the camera ($t/T = 1.31$), horizontal field exhibits energetic vortices of typical sizes of M. At larger times, we observe the persistence of large horizontal scale structures. Furthermore, vertical fields show strongly horizontally elongated structures, which is a robust feature of turbulence in stratified fluids.

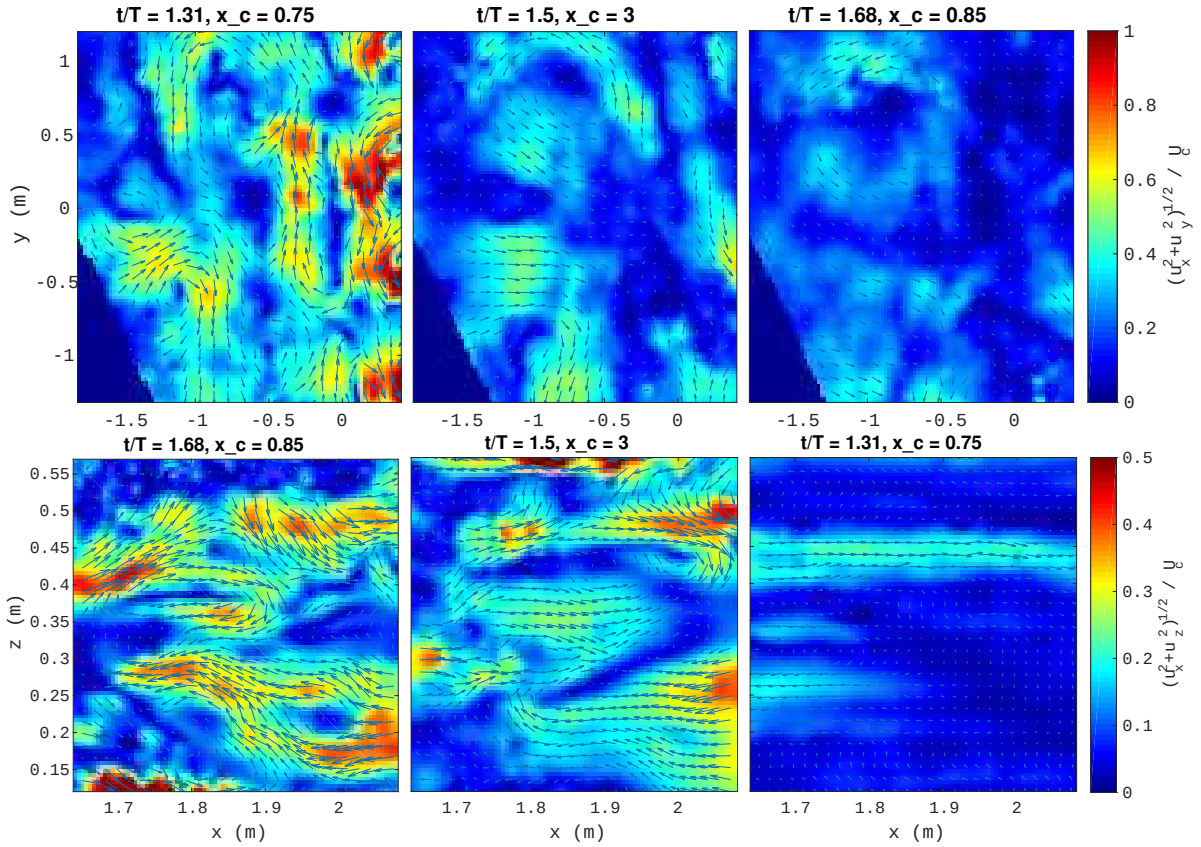

Figure 3: Instantaneous horizontal large fields (top, $z = 40$ cm) and vertical fields (bottom) for $t/T = [1.31,\ 1.5,\ 1.68]$, $F_{hc} = 0.1$ and $\mathcal{R}_c = 450$. Background colors indicate the norm of the 2D field normalized by U_c, which is $(u_x^2 + u_y^2)/U_c$ and $(u_x^2 + u_z^2)/U_c$, respectively.

3 Preliminary results for $F_{hc} = 0.1$ and $\mathcal{R}_c = 450$

With this setup, energy is injected locally by an oscillating comb of cylinders. Turbulence in a given region of interest is therefore inhomogeneous and unstationary. Evolution of kinetic energy with time is then an important feature of this flow. Figure 4 represents the normalized horizontal kinetic energy $\langle u_x^2 + u_y^2 \rangle / 2U_c^2$ as a function of the fractional part of normalized time $\{t/T\}$ for 5 particular periods, with $\langle \cdot \rangle$ denoting 3D spatial average. Kinetic energy is computed from large horizontal PIV fields for each time when the carriage does not appear in the field of view of the camera. The carriage is stopped at the end of the 12th period. The flow undergoes successive turbulent decays. The energy injects is of the order of $U^2 \simeq 0.08 U_c^2$. We estimate the mean kinetic energy dissipation rate to $\varepsilon_K \simeq 2 \times 10^{-2} U_c^3 / M$ by computing the time average of $-\partial \langle u_x^2 + u_y^2 \rangle / \partial t$ over $0.3 < \{t/T\} < 0.35$.

We now characterize the distribution of energy among scales by second-order structure function, defined as

$$S_h(r) = (S_{xx} + S_{yy} + S_{xy} + S_{yx})/2, \tag{4}$$

$$\text{with} \quad S_{ij} = \langle \overline{(u_i(\mathbf{x} + r\mathbf{e}_j) - u_i(\mathbf{x}))^2} \rangle, \tag{5}$$

and $\bar{\cdot}$ time average when the carriage is moving. For a developed turbulence, and for scales larger than the dissipative scale and lower than injection scale, we expect $S_h(r) = C(\varepsilon r)^{2/3} = C'(r U_c^3 / M)^{2/3}$, with C a coefficient approximately equal to 6 (see figure 15 in Augier et al., 2015). Figure 5 represents normalized second-order structure function

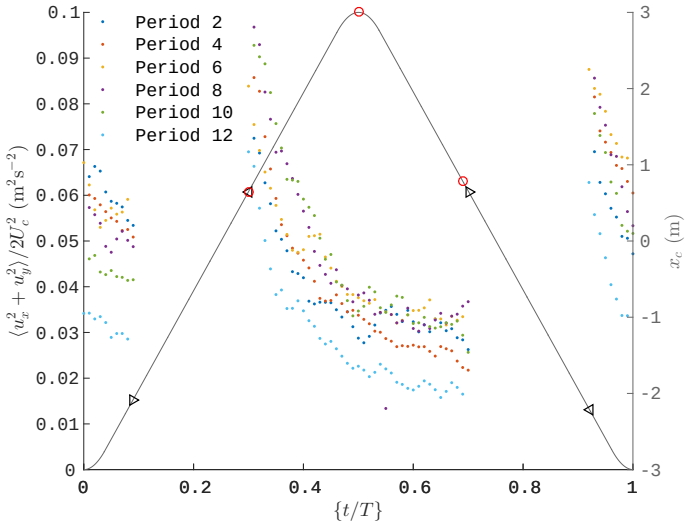

Figure 4: Spatial average of normalized horizontal kinetic energy $\langle u_x^2 + u_y^2 \rangle / 2U_c^2$ as a function of the fractional part of the normalized time $\{t/T\}$ for different periods of measurement and for $F_{hc} = 0.1$ and $\mathcal{R}_c = 450$. Times where no data appears corresponds to those when the carriage is in the field of view and hides a part of the field of view. The gray line represents the position of the carriage x_c and the three red circles mark the times chosen for the figure 3. The pair of symbols $\triangleleft - \triangleright$ delimits the ranges of time where the carriage appears in the field of view.

computed from large horizontal fields for a 12 periods forcing experiment. Interestingly, the curve exhibits a plateau corresponding to a $r^{2/3}$ scaling law on half a decade at a value going from 0.4 at $\{t/T\} = 0.31$ to 0.2 at $\{t/T\} = 0.31$. Supposing that this range corresponds to an inertial range, we evaluate a surrogate of the mean dissipation rate at $\varepsilon_K \sim 0.01 U_c^3/M$. This order of magnitude is consistent with the previous estimation by direct computation of the energy decay.
By extrapolation of the energy dissipation rate and energy injected at the vicinity of the carriage, we define surrogates of the turbulent horizontal Froude and buoyancy Reynolds numbers based on the measured flow as

$$F_{he} \simeq \frac{\varepsilon_K}{NU^2} \simeq 0.25 F_{hc}, \quad \mathcal{R}_e \simeq \frac{\varepsilon_K}{\nu N^2} \simeq 2 \times 10^{-2} \mathcal{R}_c. \tag{6}$$

For this case for $F_{hc} = 0.1$ and $\mathcal{R}_c = 450$, we find $F_{he} \simeq 0.02$ and $\mathcal{R}_e \simeq 9$. These orders of magnitude correspond to flows for which a downscale energy cascade and horizontal spectra with a -5/3 scaling law have been observed numerically (Brethouwer et al., 2007; Augier et al., 2015). This strongly indicates that the $r^{2/3}$ scaling law for S_h is indeed related to strongly stratified turbulence.
The values of these dimensionless parameters given in table 1 for the other cases show that we were able with this experiment setup to span very interesting ranges of parameters, from very strongly stratified ($F_{he} \simeq 0.01$) to weakly stratified ($F_{he} \simeq 0.1$) and from small to large buoyancy Reynolds numbers. Although the analysis of the data is still at a very preliminary stage, the reached values of the turbulent numbers F_{he} and $\mathcal{R}_e$ will enable us to address the question of mixing efficiency in the regime relevant of the ocean dynamics.

Acknowledgements

This project has received funding from the foundation Simone et Cino Del Duca de l'Institut de France and the European Research Council (ERC) under the European

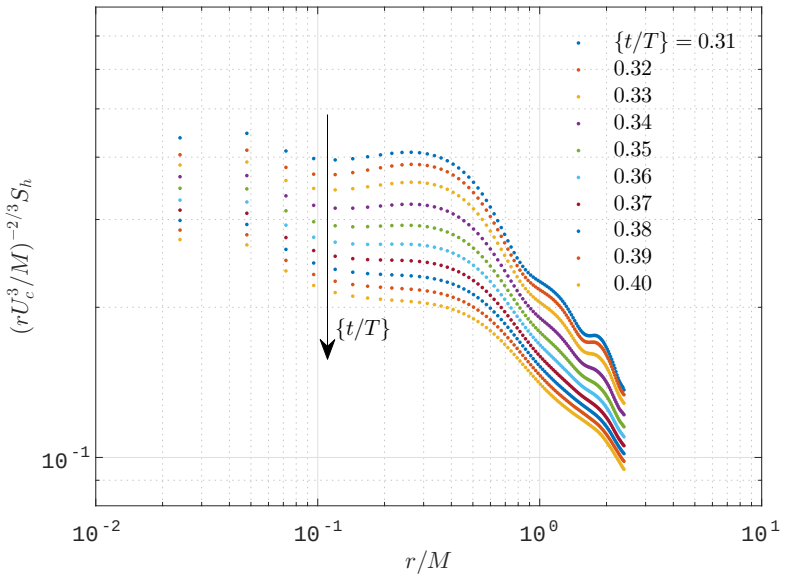

Figure 5: Normalized second-order structure S_h function as a function of r/M for $F_{hc} = 0.1$ and $\mathcal{R}_c = 450$.

Union's Horizon 2020 research and innovation program (grant agreement No 647018-WATU and Euhit consortium). We thank Mile Kusulja, Thomas Valran, Julie Germinario and Gabriel Moreau for their help to design, build and carry out this experiment.

References

Augier, P., Billant, P., and Chomaz, J.-M. (2015). Stratified turbulence forced with columnar dipoles. numerical study. *J. Fluid Mech.*, 769:403–443.

Augier, P., Billant, P., Negretti, M. E., and Chomaz, J.-M. (2014). Experimental study of stratified turbulence forced with columnar dipoles. *Phys. Fluids*, 26(4).

Billant, P. and Chomaz, J.-M. (2001). Self-similarity of strongly stratified inviscid flows. *Physics of Fluids*, 13:1645.

Brethouwer, G., Billant, P., Lindborg, E., and Chomaz, J.-M. (2007). Scaling analysis and simulation of strongly stratified turbulent flows. *J. Fluid Mech.*, 585:343–368.

Brethouwer, G. and Lindborg, E. (2009). Numerical study of vertical dispersion by stratified turbulence. *J. Fluid Mech.*, 631:149–163.

Lindborg, E. (2006). The energy cascade in a strongly stratified fluid. *J. Fluid Mech.*, 550:207–242.

Maffioli, A. and Davidson, P. A. (2016). Dynamics of stratified turbulence decaying from a high buoyancy Reynolds number. *J. Fluid Mech.*, 786:210–233.

Praud, ., Fincham, A., and Sommeria, J. (2005). . *J. Fluid Mech.*, 631:149–163.

Riley, J. J. and de Bruyn Kops, S. M. (2003). Dynamics of turbulence strongly influenced by buoyancy. *Phys. Fluids*, 15(7):2047–2059.

Riley, J. J. and Lindborg, E. (2008). Stratified Turbulence: A Possible Interpretation of Some Geophysical Turbulence Measurements. *J. Atmos. Sci.*, 65:2416–2424.